Biosensors and Bioelectronics 209 (2022) 114243

Contents lists available at ScienceDirect

Biosensors and Bioelectronics

journal homepage: www.elsevier.com/locate/bios

Electrical monitoring of infection biomarkers in chronic wounds using nanochannels

Alba Iglesias-Mayor [a], Olaya Amor-Gutiérrez [a], Celia Toyos-Rodríguez [a], Arnau Bassegoda [b], Tzanko Tzanov [b], Alfredo de la Escosura-Muñiz [a,c,*]

[a] NanoBioAnalysis Group - Department of Physical and Analytical Chemistry, University of Oviedo, Julián Clavería 8, 33006, Oviedo, Spain
[b] Grup de Biotecnologia Molecular i Industrial, Department of Chemical Engineering, Universitat Politècnica de Catalunya, Terrassa, Spain
[c] Biotechnology Institute of Asturias, University of Oviedo, Santiago Gascon Building, 33006, Oviedo, Spain

ARTICLE INFO

Keywords:
Nanopores
Nanochannels
Wound infection
Lysozyme
Peptidoglycan
Electrochemical detection

ABSTRACT

Chronic wounds represent an important healthcare challenge in developed countries, being wound infection a serious complication with significant impact on patients' life conditions. However, there is a lack of methods allowing an early diagnosis of infection and a right decision making for a correct treatment. In this context, we propose a novel methodology for the electrical monitoring of infection biomarkers in chronic wound exudates, using nanoporous alumina membranes. Lysozyme, an enzyme produced by the human immune system indicating wound infection, is selected as a model compound to prove the concept. Peptidoglycan, a component of the bacterial layer and the native substrate of lysozyme, is immobilized on the inner walls of the nanochannels, blocking them both sterically and electrostatically. The steric blocking is dependent on the pore size (20–100 nm) and the peptidoglycan concentration, whereas the electrostatic blocking depends on the pH. The proposed analytical method is based on the electrical monitoring of the steric/electrostatic nanochannels unblocking upon the specific degradation of peptidoglycan by lysozyme, allowing to detect the infection biomarker at 280 ng/mL levels, which are below those expected in wounds. The low protein adsorption rate and thus outstanding filtering properties of the nanoporous alumina membranes allowed us to discriminate wound exudates from patients with both sterile and infected ulcers without any sample pre-treatment usually indispensable in most diagnostic devices for analysis of physiological fluids.

Although size and charge effects in nanochannels have been previously approached for biosensing purposes, as far as we know, the use of nanoporous membranes for monitoring enzymatic cleavage processes, leading to analytical systems for the specific detection of the enzymes has not been deeply explored so far. Compared with previously reported methods, our methodology presents the advantages of no need of neither bioreceptors (antibodies or aptamers) nor competitive assays, low matrix effects and quantitative and rapid analysis at the point-of-care, being also of potential application for the determination of other protease biomarkers.

1. Introduction

Healing of chronic wounds, affecting 1 to 2 percent of the population in developed countries, represents a major healthcare challenge with important financial burden (Clinton and Carter, 2015) (Järbrink et al., 2016). Chronic wounds are usually heavily colonized with bacteria, while providing bacteria-free environment is a prerequisite for wound healing. An early detection and treatment of infection is one of the most important factors in wound management. Although classical signs of infection - like redness, heat, swelling, exudate production and pain (Gardner et al., 2001) - are still the main criteria in the clinical examination of the wound status, they are ambiguous and depend on the experience of the healthcare practitioner (Siddiqui and Bernstein, 2010). More precise, but still questioned are the (semi)quantitative microbiological investigations, including the gold-standard biopsy method, a time-consuming technique which is not often carried out in ambulatory clinical practice to avoid patient's morbidity, mostly local bleeding and infection spread (Gardner et al., 2006). The correct microbiological identification of the microorganisms infecting a wound in order to prescribe the suitable antibiotic treatment may take up to 3

* Corresponding author. NanoBioAnalysis Group - Department of Physical and Analytical Chemistry, University of Oviedo, Julián Clavería 8, 33006, Oviedo, Spain.
E-mail address: alfredo.escosura@uniovi.es (A. Escosura-Muñiz).

https://doi.org/10.1016/j.bios.2022.114243
Received 8 March 2022; Received in revised form 30 March 2022; Accepted 1 April 2022
Available online 5 April 2022

days to come from the Microbiology lab in many hospitals. Until then, the patient is subjected to a broad-spectrum unspecific antimicrobial therapy with important side effects on human microbiome. For this reason, alternative tools for the rapid detection of infections in chronic wounds are strongly required.

Although physical parameters such as temperature (Matzeu et al., 2011), pH (Trupp et al., 2010) or odour (Persaud, 2005) have been studied as qualitative indicators of wound infection (Cutting and White, 2005) (Caliendo et al., 2013), main efforts have been dedicated in the last decades to the identification of biomolecules which presence in wound exudates evidences a bacterial infection (Yager et al., 2007). Enzymes with increased activity in infected wound fluids are considered as reliable infection biomarkers (Schiffer et al., 2015). Lysozyme (Hasmann et al., 2011) is of special relevance, since it is produced by the human immune system as the main component of the host innate defence mechanism (Osserman et al., 1973). Lysozyme is a glycosidase enzyme (Callewaert and Michiels, 2010) capable of hydrolysing the β-(1, 4)-glycosidic bonds between N-acetylmuramic acid and N-acetylglucosamine residues of its native substrate, the peptidoglycan (Salton, 1957), a polymer which constitutes the core component of almost all bacterial cell walls (Rogers et al., 2013). This polymer is composed of linear glycan strands (alternating N-acetylglucosamine and N-acetylmuramic acid residues linked by β-(1,4) bonds) cross-linked by short peptides. Gram positive bacteria have a thick peptidoglycan layer and no outer lipid membrane whilst Gram negative bacteria have a thin peptidoglycan layer and an outer lipid membrane (Vollmer et al., 2008). The presence of high lysozyme activity in serum and urine samples has been associated with chronic granulomatous inflammatory disorders as tuberculosis or sarcoidosis (Jain et al., 2020) and myelomonocytic leukemia (Osserman and Lawlor, 1966), respectively. Moreover, the increase in lysozyme levels in serum is an indicator of active chronic inflammation (Hasmann et al., 2011).

The analysis of lysozyme activity has been traditionally based on its lytic action against the cell wall of *Micrococcus luteus (M. lysodeikticus),* by measuring the decrease in turbidity (Shugar, 1952). However, this methodology is affected by the pH, ionic strength and matrix effects, what implies that these parameters must be thoroughly controlled to obtain a proper result (Mörsky, 1983). Colorimetric methods based on i) the release of coloured fragments of Remazol brilliant blue-labelled *Micrococcus luteus* upon hydrolysis (Ito et al., 1992) (Hardt et al., 2003) and ii) peptidoglycan stabilized-gold nanoparticles aggregation after enzymatic cleavage (Fu et al., 2018) have also been proposed for such purpose. However, these methods are laborious and require additional separation steps, having as main drawback the low contrast observed in some procedures between signal and background (Hardt et al., 2003). Chromatographic (Fang et al., 2021) and both antibody (Vidal et al., 2005) and aptamer-based (Ostatná et al., 2017) methods have also been reported for lysozyme detection, suffering from important limitations related to their high cost and the need of bioreceptors.

Biosensing systems based on nanochannels emerge as outstanding tools to overcome these limitations and meet such clinical demand. The use of nanopores/nanochannels has become one of the most promising fields of research in the biosensing area in the last years (de la Escosura-Muñiz and Merkoçi, 2012). Proteins, DNA sequences and viruses have been detected through the so-called stochastic sensing on single natural/artificial nanopores. Special mention deserves the commercial implementation of DNA sequencing systems based on the same principles (Clarke et al., 2009). Nanoporous membranes have also been proposed as platforms for both electrochemical and optical biosensing through the monitoring of the nanochannels steric blockage upon biocomplex formation (de la Escosura-Muñiz and Merkoçi, 2016). The easy functionalization and capacity for mass production of nanoporous alumina have made this material as the most extensively used for such applications (Losic and Santos, 2015). Size and charge effects in nanochannels have been approached for biosensing purposes for more than ten years (Li et al., 2010) (Wang et al., 2012) (Yu et al., 2014) (Wang et al., 2016) (Zhou et al., 2020). However, the use of nanoporous membranes for monitoring enzymatic cleavage processes, leading to analytical methods for enzyme determination has not been deeply explored so far.

In this context, we propose a novel methodology for the determination of lysozyme using nanoporous alumina membranes as sensing platforms and indium tin oxide/poly(ethylene terephthalate) (ITO/PET) electrodes as transducers. This analytical method is based on the electrical monitoring of steric/electrostatic nanochannels blocking upon peptidoglycan immobilization and further lysozyme digestion of the peptidoglycan leading to unblockage of the nanopores. Steric and electrostatic contributions to the nanopore blocking/unblocking mechanism are thoroughly studied, before analysing samples of wound exudates from both patients with clean and infected ulcers.

Our novel methodology presents important advantages compared with the lysozyme detection methodologies reported so far, related to: i) no need of bioreceptors (antibodies or aptamers); ii) no need of competitive assays; iii) low matrix effects thanks to the filtering-like properties and low protein adsorption rate of the nanoporous alumina membranes; iv) quantitative analysis and v) rapid analysis at the point-of-care, using cheap and portable instruments.

2. Experimental section

2.1. Chemicals and equipment

(3-aminopropyl) triethoxysilane (APTES), *N*-(3-Dimethylaminopropyl)-*N′*-ethylcarbodiimide hydrochloride (EDC), *N*-Hydroxysulfosuccinimide sodium salt (sulfo-NHS), peptidoglycan from *Bacillus subtilis,* lysozyme from chicken egg white, bovine serum albumin (BSA), avidin from egg white and potassium ferrocyanide $K_4[Fe(CN)_6]$ were purchased from Sigma-Aldrich (Spain). Hyaluronidase (HYAL) has been purchased from MyBioSource (USA). Lysozyme ELISA Kit used for sample validation was provided by Abcam (UK). Red-ox indicator media used for the electrochemical measurements consisted in 10 mM $K_4[Fe(CN)_6]$ solutions prepared in different buffers: 0.1 M sodium acetate pH 4.5, 0.1 M MES (2-(*N*-morpholino) ethanesulfonic acid) pH 6.5, and 0.1 M Tris (tris(hydroxymethyl) aminomethane)-HCl pH 7.2. Unless otherwise specified, all buffer reagents and other inorganic chemicals of analytical grade were supplied by Sigma-Aldrich (Spain) and used without further purification. The solutions were prepared in ultrapure water (18.2 MΩ cm @ 25 °C) obtained with a Millipore Direct-Q® 3 UV purification system from Millipore Ibérica S.A (Spain).

Anodic aluminum oxide (alumina) nanoporous membranes (Whatman® Anodisc™ filters, 13 mm diameter, 60 μm thickness, containing 20, 100 or 200 nm pores) and indium tin oxide coated poly(ethylene terephthalate) (ITO/PET) sheets (surface resistivity 60 Ω/sq) were purchased from Sigma-Aldrich (Spain). The electrochemical transducers were ITO/PET pieces of 43 × 20 mm, defining a working electrode of 8 mm in diameter. Reference and counter electrodes were made of silver/silver chloride (CH Instruments, Inc.; United States of America) and of a platinum wire (Alfa Aesar; United States of America) respectively. A methacrylate electrochemical cell was used for the electrochemical measurements that were performed with an Autolab PGSTAT-10 from Eco Chemie (Netherlands), controlled by Autolab GPES software, connected to a PC. All measurements were carried out at room temperature with a working volume of 400 μL. A SANYO MIR-262 incubator purchased from SANYO Electric Co. Ltd. (Japan) was used for the enzymatic incubations with lysozyme at 37 °C. Nanoporous membranes used in this work have been characterized by scanning electron microscopy (SEM). Scanning electron microscopy images were obtained using a JEM-6610 from JEOL (Japan) with an accelerating voltage of 20 kV.

Swabs with exudates from patients with potentially non-infected and infected skin ulcers were provided by the Chronic Ulcers Unit of the Hospital Universitario Central de Asturias (HUCA).

2.2. Methods

2.2.1. Nanoporous alumina membranes functionalization, peptidoglycan immobilization and enzymatic cleavage by lysozyme

Peptidoglycan immobilization on the inner walls of the nanochannels was performed adapting an experimental procedure previously optimized for antibodies (de la Escosura-Muñiz and Merkoçi, 2011). It consists first in the generation of amino groups in the nanochannels *via* silanization, followed by carbodiimide-mediated peptidoglycan binding through its carboxyl groups. Briefly, nanoporous alumina membranes were first boiled in ultrapure water for 1 h, so as to clean the membranes and the hydroxyl groups of the alumina, which favour the later silanization process (Ye et al., 2016). After drying in nitrogen, they were immersed in a 5% acetone solution of APTES for 1 h. Then, membranes were washed in acetone and baked at 120 °C for 30 min. After that, 30 μL of peptidoglycan solution in 10 mM MES pH 5 buffer, containing 5 mM EDC/sulfo-NHS, were placed on the filtering side of the membrane and left there for 2 h. A scheme illustrating this procedure is shown at the Supporting Information (Figure S1).

After thoroughly washing with 10 mM Tris-HCl (10 mM ionic strength coming from NaCl) pH 8 buffer, the enzymatic reaction was performed by incubating 30 μL of lysozyme solution (concentration range from 1 to 50 μg/mL) in 10 mM Tris-HCl pH 8 on the membrane filtering side at 37 °C for 30 min. Finally, the membranes were washed again and stored in the measurement buffer before the electrochemical experiments. Control assays were performed following the same protocol but using 10 mM phosphate buffered saline (PBS) pH 7.4 solution instead of peptidoglycan solution (bare silanized nanoporous membranes). Three exudates from clean wound ulcers and three from infected ulcers were analysed following the same experimental procedure but using a 1 to 10 dilution (in 10 mM Tris-HCl pH 8) of the wound exudate instead of lysozyme solution.

Selectivity assays were performed following the same experimental procedure but using a 25 μg/mL concentration of avidin, HYAL and BSA. The long-term stability of the peptidoglycan-modified membranes was evaluated by storing a set of them (peptidoglycan concentration: 5 mg/mL) at 4 °C for one month. The nanochannel blocking was evaluated in different days during this period.

2.2.2. Nanoporous cell set-up and electrochemical detection

The design of the experimental set-up for the electrochemical detection using nanoporous alumina membranes is shown in Fig. 1. Nanoporous membranes were physically attached onto the ITO/PET electrode, placing it onto a methacrylate block and putting the membrane with the filtering side up over the electrode surface. Then, a second block containing a hole of 8 mm in diameter was placed onto the membrane, with an insulating O-ring between them to avoid liquid leakage. Finally, the system was fixed with screws, defining an electrochemical cell that was filled with the 10 mM $K_4[Fe(CN)_6]$ red-ox indicator solution. All measurements were carried out with a working volume of 400 μL, which was enough to cover the three-electrode system (silver/silver chloride reference electrode, platinum wire counter electrode and ITO/PET working electrode).

A pre-treatment at −0.1 V was applied for 30 s and, immediately after, a differential pulse voltammetric (DPV) scan was performed from −0.1 V to +1.1 V (step potential: 10 mV, modulation amplitude: 50 mV, and scan rate: 20.1 mV/s), resulting in a voltammetric signal due to oxidation of $[Fe(CN)_6]^{4-}$ to $[Fe(CN)_6]^{3-}$, which peak current at approximately +0.40 V was chosen as the analytical signal. The measurements were carried out in triplicate at room temperature under non-stirring conditions. Each measurement was performed with a single nanoporous membrane and an ITO/PET electrode, discarded after the measurement.

3. Results and discussion

3.1. Nanochannels blockage by peptidoglycan: steric and electrostatic contributions

As illustrated in Fig. 2, it is envisaged that the immobilization of peptidoglycan in the nanochannels produces a blockage in the diffusion of the electroactive species through the nanoporous membranes to the electrochemical transducer surface. Furthermore, it is also expected that the degradation of peptidoglycan by lysozyme will lead to the unblockage of the nanopores.

Such nanochannels blocking after peptidoglycan immobilization can be attributed to a dual effect based on both steric and charge repulsion effects. Considering the size of both peptidoglycan (around 10 nm) (Tulum et al., 2019) and $[Fe(CN)_6]^{4-}$ red-ox indicator ions (<1 nm), it is expected that in absence of peptidoglycan the red-ox ions can freely flow through the nanochannel to the electrode, whereas the presence of peptidoglycan will hinder their passage due to steric impairments.

On the other hand, it is worthy to note that the peptidoglycan can be negatively charged, positively charged or without a net charge depending on the pH of the measurement buffer solution. Peptidoglycan electronic charge may influence the nanopores blockage due to charge repulsion effects. If the peptidoglycan is negatively charged (working at a pH higher than peptidoglycan's isoelectric point) a repulsion effect between the negative charges of the peptidoglycan and the negative ones from the red-ox indicator ions is expected. This charge repulsion will hinder the ions diffusion to the electrode.

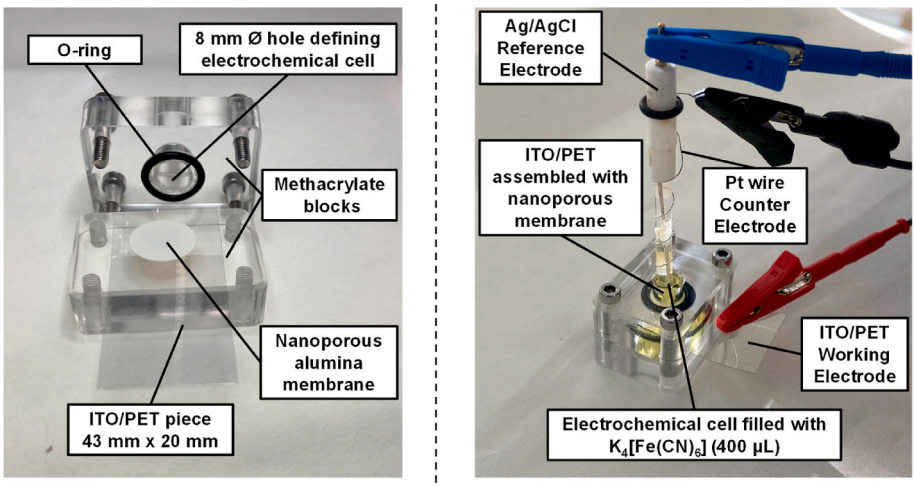

Fig. 1. Experimental set-up for the electrochemical monitoring of the blocking/unblocking of the nanoporous alumina membranes attached to ITO/PET working electrode.

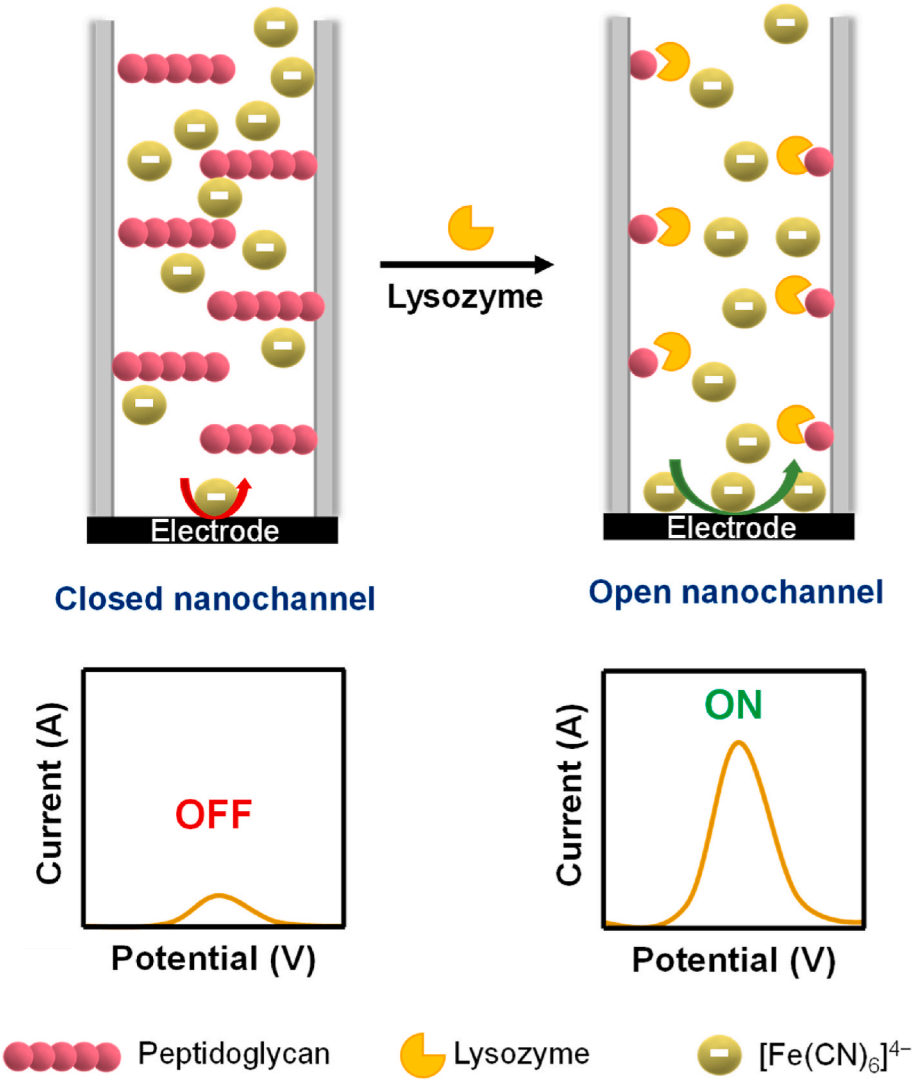

Fig. 2. Scheme (not in scale) of the biosensing system based on nanochannel steric/electrostatic blocking by peptidoglycan and further unblocking after enzymatic cleavage by lysozyme.

Therefore, before carrying out lysozyme determination, a series of optimizations were made with the aim of achieving the maximum steric/electrostatic blocking of the nanochannels by immobilizing peptidoglycan on their inner walls.

With the aim to simplify and normalize the results, in the studies shown along the following sections, the degree of blockage will be expressed in terms of % of decrease in the analytical signal, compared with the one obtained for the bare silanized membrane, calculated as follows:

$$Blockage\ (\%) = \left| \left(\frac{(i_p\ peptidoglycan\ modified\ membrane\ -\ i_p\ bare\ membrane)}{i_p\ bare\ membrane} \right) x\ 100 \right|$$

3.1.1. Effect of the peptidoglycan concentration

The effect of peptidoglycan concentration on the nanochannels blockage and thus on the analytical signal was first studied with membranes containing nanopores of 20 nm. Peptidoglycan from solutions at different concentrations (1 and 5 mg/mL) was immobilized in the nanochannels through carbodiimide chemistry, as detailed in the methods section. The nanochannels blocking was evaluated by the voltammetric monitoring of the diffusion of the $[Fe(CN)_6]^{4-}$ ions in buffer at pH 7.2.

As shown in Fig. 3A, when increasing the amount of peptidoglycan in the nanochannels, the $[Fe(CN)_6]^{4-}$ ions diffusion is hindered, probably due to both steric and electrostatic effects, leading to a decrease in the voltammetric signal from the oxidation of $[Fe(CN)_6]^{4-}$ to $[Fe(CN)_6]^{3-}$. As summarized in Fig. 3B, the 18% blocking in the signal recorded at 1 mg/mL peptidoglycan increased up to 47% when using 5 mg/mL peptidoglycan. Higher concentrations were not assayed for cost saving considerations. In view of these results, a peptidoglycan concentration of 5 mg/mL was selected as the optimum for the biosensor development.

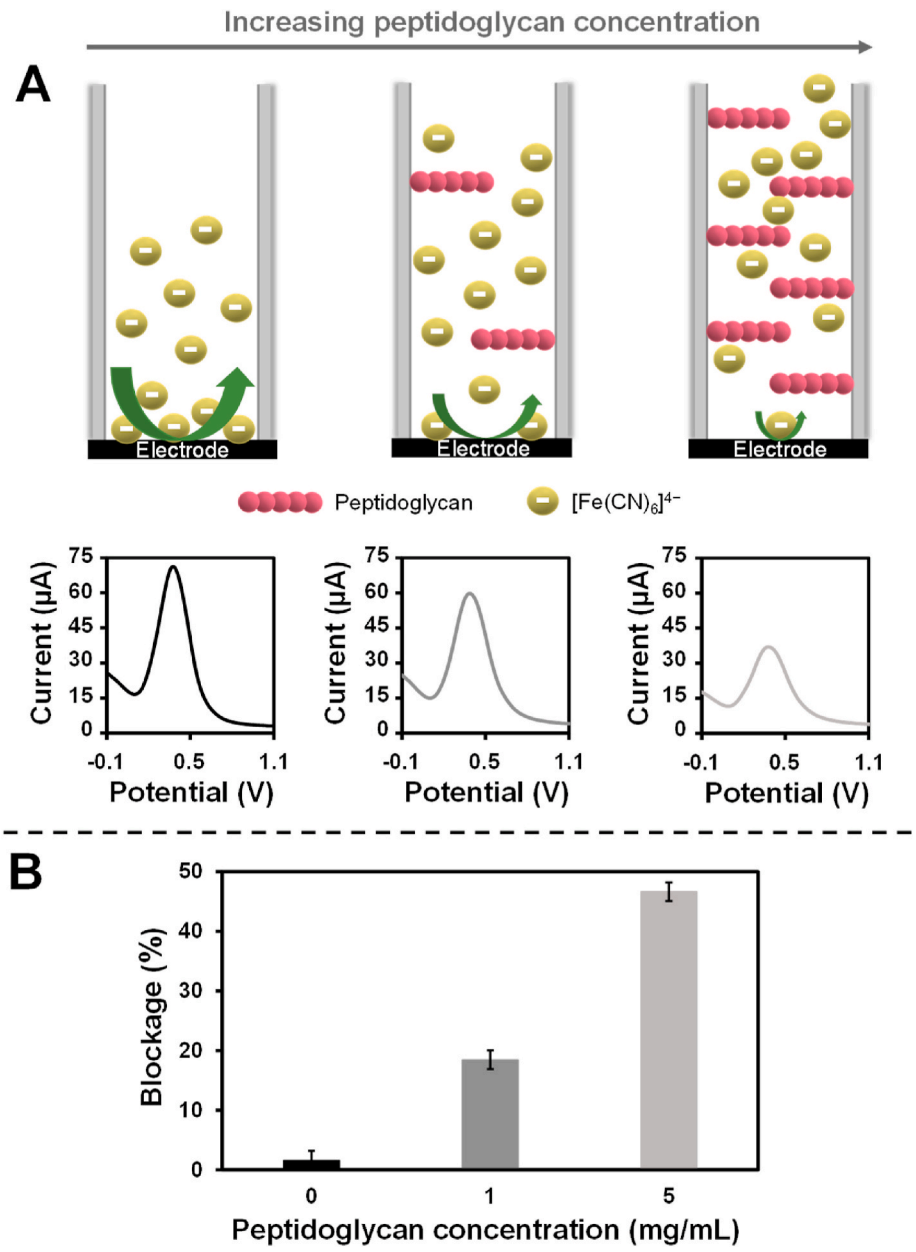

Fig. 3. Effect of the peptidoglycan concentration on the nanochannels blockage. (A) Schematic illustration of the different amount of immobilized peptidoglycan, and its effect on the $[Fe(CN)_6]^{4-}$ ions diffusion to the electrode. Differential pulse voltammograms registered in 10 mM $K_4[Fe(CN)_6]$/0.1 M (in buffer at pH 7.2) for nanoporous membranes (20 nm pore size), bare silanized (left) and modified with 1 mg/mL (middle) and 5 mg/mL (right) of peptidoglycan. DPV parameters: pre-concentration potential: -0.1 V; pre-concentration time: 30 s; step potential: 10 mV, modulation amplitude: 50 mV, and scan rate: 20.1 mV/s. (B) Comparative bar chart of the signal blockage (expressed in percentage) for different peptidoglycan concentrations. Data are given as average ± SD (n = 3).

3.1.2. Effect of the pH: electrostatic forces involved in nanochannels blocking

pH is a key parameter affecting the ionic transport in nanochannels (Gao et al., 2013) (Li et al., 2013) (Li et al., 2014) (Li et al., 2015) (Zhao et al., 2019). In our particular case, the pH of the measurement buffer solution drives the peptidoglycan electronic charge, affecting the electrostatic forces involved in the nanochannels blocking. Considering the isoelectric point of the peptidoglycan (pI: 6.5) (Yoshida et al., 1996), solutions of the 10 mM $K_4[Fe(CN)_6]$ red-ox indicator were prepared in different buffers at pH below, equal and above this value. Typical buffers for each range of pH were selected: 0.1 M NaAc (for pH 4.5), 0.1 M MES (for pH 6.5) and 0.1 M Tris-HCl (for pH 7.2). The evaluation of any of these buffers at a pH different from their typical value was not considered appropriate. Membranes containing nanopores of 20 nm, where the peptidoglycan is immobilized from a 5 mg/mL solution were used for this study.

As shown in Fig. 4, when the pH of the measurement buffer solution is higher than the pI of the peptidoglycan (pH 7.2), a high blocking (47% decrease in the signal) is observed. These experimental results are in line with the hypothesis about the effect of the nanochannel charges on the diffusion of $[Fe(CN)_6]^{4-}$ anions, which has also been proposed by other authors (Li et al., 2010). At this pH the peptidoglycan is negatively charged, and such charges attract cations and repel anions, forming a negatively charged electric field, also called electrostatic repulsion region. Such restriction region decreases the lane for anions, resulting in a decreased flux of $[Fe(CN)_6]^{4-}$ and consequently a lower voltametric signal, what we call a high blockage. However, when working below the pI of the peptidoglycan (pH 4.5), it is positively charged and the situation is the opposite: a positively charged electric field is generated, favoring the pass of $[Fe(CN)_6]^{4-}$ anions for keeping neutral charge in the nanochannel, leading to a higher voltametric signal, what we call a low blockage (5% decrease in the signal). At pH of the red-ox indicator medium equal to the pI of the peptidoglycan (pH 6.5), the peptidoglycan molecules are uncharged and the $[Fe(CN)_6]^{4-}$ ions diffusion through the nanochannel is neither electrostatically favored nor hindered, obtaining a 15% of signal blockage, probably only due to steric issues.

Considering these findings, in further experiments the electrochemical measurements were performed at the maximum electrostatic

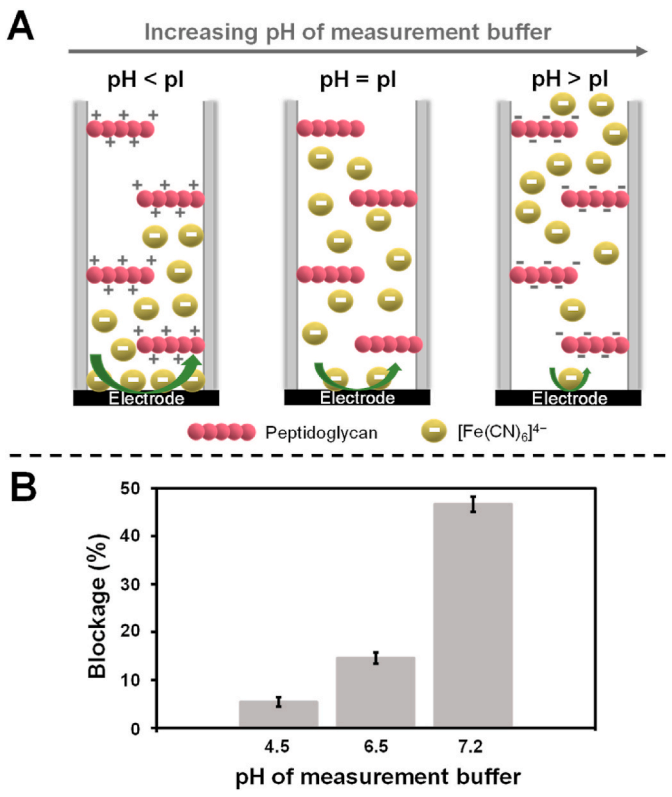

Fig. 4. Measurement buffer pH effect on the nanochannels blockage. (A) Schematic illustration of the different net charge of the peptidoglycan (pI: 6.5) depending on the pH of the measurement buffer, and its effect on the $[Fe(CN)_6]^{4-}$ ions diffusion to the electrode. (B) Comparative bar chart of the signal blockage (expressed in percentage) for measurement buffer solutions at different pH. Data are given as average ± SD (n = 3). Peptidoglycan concentration: 5 mg/mL. $K_4[Fe(CN)_6]$ concentration: 10 mM (at different pH measurement buffer solutions).

blockage conditions, that is using a buffer at pH 7.2 as red-ox indicator medium solution.

3.1.3. *Effect of the nanopore size*

The steric blockage of the nanochannels will depend not only on the peptidoglycan concentration but also on the nanopore size, expecting a lower degree of blockage when increasing the nanopore size. Nanoporous membranes containing nanopores of 20 nm, 100 nm and 200 nm were evaluated for such purpose. A peptidoglycan concentration of 5 mg/mL and a red-ox indicator medium solution at pH 7.2 were fixed for this study.

As schematized in Fig. 5A, for the smaller nanopore size (20 nm) the peptidoglycan molecules in the opposite walls of the nanochannels are very close, and this proximity leads to a steric blockage that prevents the flow of $[Fe(CN)_6]^{4-}$ ions. However, when increasing the nanopore size, the distance between the nanochannel walls increases, which facilitates the ions' flow, leading to a decrease in the steric blockage.

From the obtained results (Fig. 5B) it can be concluded that the higher is the nanopore size, the lower the steric blockage. The blocking percentage found for the 20 nm membranes (47%) decreases to 17% when using the intermediate nanopore size (100 nm) membranes, and further to 6% for the higher nanopore size (200 nm) membranes. In line with these results, nanoporous membranes containing pores of 20 nm, for which the maximum signal blocking by the peptidoglycan was achieved, were chosen for lysozyme sensing.

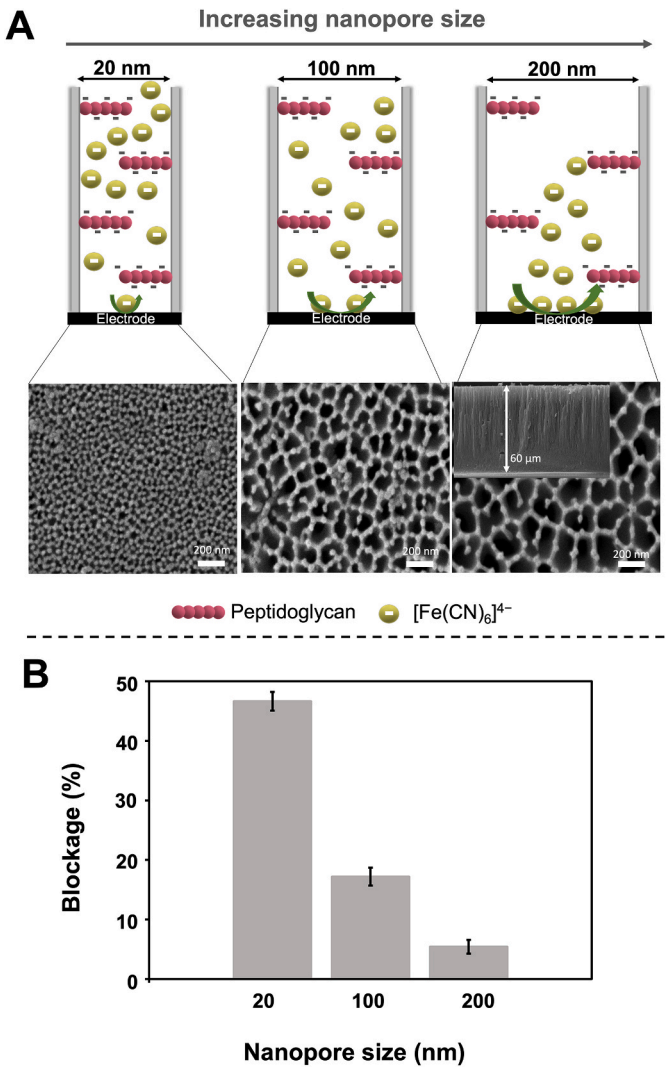

Fig. 5. Effect of the nanopore size on the nanochannels blockage. (A) Schematic representation of the effect of different nanopore sizes on the $[Fe(CN)_6]^{4-}$ ions diffusion to the electrode, together with SEM top-view micrographs of the nanoporous membranes. The inset in the image of the 200 nm-pores membrane corresponds to a cross-section view. (B) Comparative bar chart of the signal blockage (expressed in percentage) for nanoporous membranes with different nanopore sizes. Data are given as average ± SD (n = 3). Peptidoglycan concentration: 5 mg/mL. $K_4[Fe(CN)_6]$ concentration: 10 mM (in buffer at pH 7.2).

3.2. *Electrochemical detection of lysozyme*

As previously detailed (Fig. 2), the proposed sensing system is based on the specific cleavage of the β-(1,4)-glycosidic bonds of the peptidoglycan by lysozyme, which leads to the unblockage of the nanochannels. For this purpose, the peptidoglycan-modified membranes were incubated with lysozyme (concentration range from 1 to 50 µg/mL) at the optimum conditions for the enzymatic reaction (37 °C, 30 min) (Sambrook et al., 1989).

As expected (Fig. 6A), the voltammetric signal obtained for the peptidoglycan-modified membranes (blue continuous line) gradually increases with the amount of lysozyme (dotted lines), evidencing the unblockage of the nanochannels by specific degradation of the peptidoglycan. As a result, the analytical signal ($[Fe(CN)_6]^{4-}$ oxidation peak current at +0.40 V) increases with the lysozyme concentration in the range 0–50 µg/mL. Both parameters are adjusted to a linear relationship in the range 0-10 µg/mL (Fig. 6B), with a correlation coefficient of 0.9994, according to the following equation:

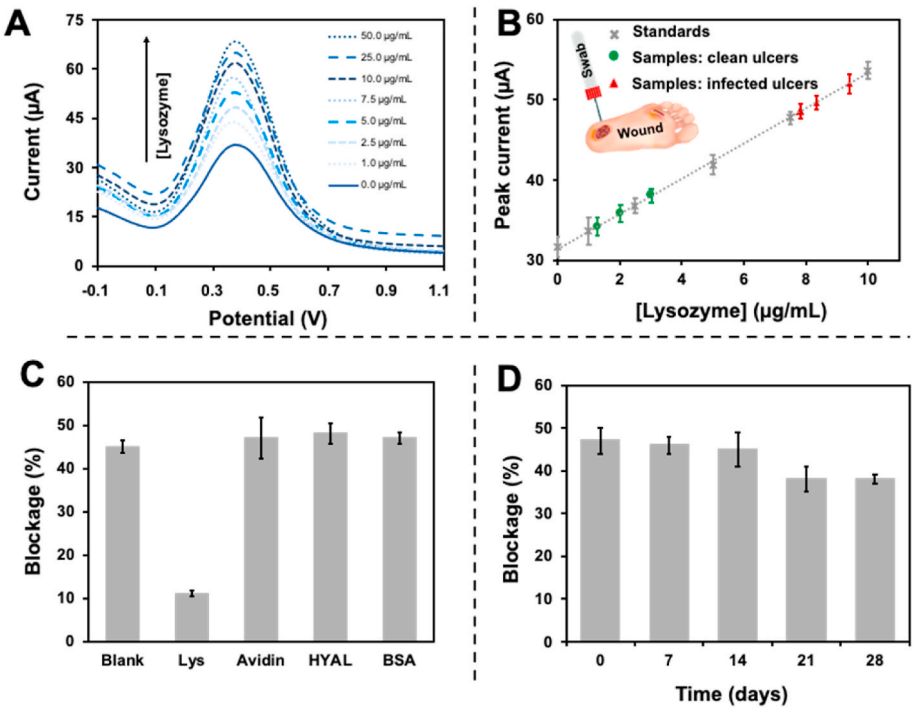

Fig. 6. Lysozyme determination through the enzymatic cleavage of peptidoglycan, leading to nanochannels unblockage. (A) Differential pulse voltammograms registered in 10 mM $K_4[Fe(CN)_6]$/0.1 M (in buffer at pH 7.2) for 5 mg/mL peptidoglycan-modified membranes (20 nm nanopores) after incubation with increasing concentrations of lysozyme (0–50 μg/mL, from down to up). DPV parameters: pre-concentration potential: -0.1 V; pre-concentration time: 30 s; step potential: 10 mV, modulation amplitude: 50 mV, scan rate: 20.1 mV/s. (B) Calibration plot obtained for standard solutions of lysozyme as well as the analytical signals obtained for swab exudates (diluted 1:10) from three patients with potentially clean ulcers and three patients with clearly infected ones. Data are given as average ± SD (n = 3). (C) Selectivity study of lysozyme (Lys) detection, evaluated against avidin, hyaluronidase (HYAL) and bovine serum albumin (BSA) (proteins concentration 25 μg/mL). (D) Long-term stability study of the peptidoglycan-modified membranes (Peptidoglycan concentration: 5 mg/mL).

$$\text{Peak current } (\mu A) = 2.2\ [\text{Lysozyme}]\ (\mu g/mL) + 31$$

The method shows a good reproducibility, with a relative standard deviation (RSD) of 5% (n = 3). A limit of detection (LOD, calculated as three times the standard deviation of the intercept divided by the slope) of 280 ng/mL of lysozyme was found. This value is in agreement with the obtained by standard ELISA assays (260 ng/mL) (Vidal et al., 2005), being our method considerably simpler, faster and cheaper, without the need of labels or competitive immunoassay formats. This LOD is low enough for detecting lysozyme in wounds, whose concentration is expected to be at μg/mL levels (Hasmann et al., 2011).

Moreover, the developed methodology presents improved characteristics weight up against other previously reported procedures for lysozyme detection in terms of complexity, assay time, assay cost and point-of-care suitability (Table 1). Although some of the alternative approaches also show low cost and low complexity features, the shorter assay time and the miniaturization/portability of the materials and instruments involved in our nanochannels-based sensing system makes it outstanding for point-of-care analysis.

3.3. System selectivity and stability

The selectivity of our system against other proteins that are commonly present in wound exudates, such as avidin, hyaluronidase (HYAL) and bovine serum albumin (BSA) (at a concentration of 25 μg/mL), was evaluated. As shown in Fig. 6C, no significant changes in the nanopore blockage were noticed for any of such proteins, as it is observed for lysozyme, demonstrating the excellent selectivity of the system.

The long-term stability of the peptidoglycan-modified membranes was evaluated by storing a set of them at 4 °C for one month. The nanochannel blocking was evaluated in different days during this period. As shown in Fig. 6D, the response of the system was stable and reproducible for at least 14 days, noticing a decrease in the effectivity of the immobilized peptidoglycan after 21 days of storage. The response was then stable at least after 28 days. A longer-term stability study was not considered.

3.4. Lysozyme determination in chronic wound exudates

The detection of excessive lysozyme levels in wound exudates is a sign of infection. This would allow to monitor the evolution of the healing status of the wound and to assess the effectiveness of the applied therapies.

Nanoporous alumina membranes are ideal platforms for such real application, thanks to their ability to also act as filter of biomolecules (de la Escosura-Muñiz and Merkoçi, 2011) (de la Escosura-Muñiz et al., 2013) (Espinoza-Castañeda et al., 2015), which also allows *in situ* studies on live cells and bacteria cultures (de la Escosura-Muñiz et al., 2018) (de

Table 1
Analytical characteristics of different methodologies for lysozyme detection, in terms of limit of detection (LOD), assay time, assay cost, complexity and point-of-care suitability.

Method	LOD (ng/mL)	Assay time (min)	Assay cost (estimated, €)	Complexity	Point-of-care suitability	Ref.
ELISA	260	120–240	8–15	High[a]	NO	Vidal et al. (2005)
Colorimetric lytic activity against *Micrococcus lysodeikticus*	7800	120	4–5	Medium	NO	Hasmann et al. (2011)
Peptidoglycan stabilized-gold nanoparticles aggregation	35	90–120	4–5	Low	NO	Fu et al. (2018)
Nanochannels	280	40	4–5	Low	YES	This work

[a] High complexity related to the need of a considerably number of reagents (antibodies, enzymes-substrates, etc.) and incubation/washing steps.

la Escosura-Muniz et al., 2019). It is well-known that alumina has a low protein adsorption rate, what is indeed the reason for its use as a filtering material. This filter-like property minimizes matrix effects in the analytical signal, allowing for the direct detection of lysozyme, without any pre-treatment of the sample. As detailed in the experimental section, swab exudates from three patients with potentially bacteria-free skin ulcers and three patients with infected ones were analysed following the experimental procedure previously detailed for lysozyme standard solutions. Dilution of the swab exudates to a 1:10 ratio was necessary to obtain analytical signals within the range of the calibration curve. As observed in Fig. 6B, substantially different analytical signals were obtained for infected and non-infected samples evidencing the ability of our method to discriminate them. The concentration of lysozyme in each sample was directly extrapolated from the calibration curve, taking advantage of the above detailed low matrix effects noticed when working with alumina membranes. In this way, lysozyme concentrations of 30 ± 5, 13 ± 2 and 20 ± 3 μg/mL were estimated in the clean ulcer samples while these values notably increase to 78 ± 6, 83 ± 6 and 94 ± 9 μg/mL for the infected ones. The observed behaviour correlates with the few existing literature reporting the lysozyme levels in such kind of samples (Hasmann et al., 2011) which found levels at μg/mL in both clean and infected ulcers, being notably higher for the infected ones, thus validating the feasibility of our system for the wound infection screening in a real scenario. Two of the wound exudates were also analysed by ELISA technique (see Figure S2 at the Supporting Information), providing a value of 28 μg/mL for the clean ulcer sample and 76 μg/mL for the infected one, what correlates with the values obtained by our method (30 ± 5 μg/mL and 78 ± 6 μg/mL respectively for such samples).

4. Conclusions

We have demonstrated that the infection biomarker lysozyme can be detected in chronic wound exudates using nanoporous alumina membranes, owing to the enzymatic cleavage of the peptidoglycan substrate used for blocking the alumina nanochannels. Both steric and electrostatic contributions are of key relevance for maximizing the nanochannels blocking by the substrate, which allows detecting low levels of lysozyme. Our findings suggest that while steric blocking is highly dependent on the pore size and the peptidoglycan concentration, the electrostatic blocking mainly depends on the pH of the red-ox indicator solution used for the voltammetic measurements. As far as we know, this is the first time that nanoporous membranes are used for electrochemical monitoring of enzymatic cleavage processes through the unblocking of previously blocked nanochannels, leading to an analytical method for the enzyme determination.

Our electrical method reached a lysozyme detection limit of 280 ng/mL, which is low enough for detecting lysozyme in wounds, with a good selectivity and long-term stability. This result is in line with previous reports based on ELISA assays, being our method faster and cheaper, without the need of labels or competitive immunoassay formats.

The proposed method is of particular interest for the discrimination of exudates from infected and non-infected wounds without sample pretreatment, taking advantage of the low protein absorption rate and thus outstanding filtering properties of the nanoporous alumina membranes. The increased levels of lysozyme in infected ulcer samples (around 85 μg/mL) compared with non-infected ones (around 21 μg/mL) correlate with previously reported data for wound fluids, demonstrating the feasibility of our system for the early wound infection diagnosis in the clinical scenario. Early diagnosis would allow to select a correct treatment, avoiding patients' disability and saving resources for hospitalization. Furthermore, the miniaturization and low cost of the proposed analytical methodology would allow its implementation in out-of-hospital settings as well.

Declaration of competing interest

The authors declare that they have no known competing financial interests or personal relationships that could have appeared to influence the work reported in this paper.

Acknowledgements

This work has been supported by the MCI-21-PID2020-115204RB-I00 project from Spanish Ministry of Science and Innovation (MICINN) and the SV-PA-21-AYUD/2021/51323 project from the Asturias Regional Government. A. Iglesias-Mayor thanks the Spanish Ministry of Education, Culture and Sports (MECD) for the award of a FPU Grant (FPU2014/04686). O. Amor-Gutiérrez and A. de la Escosura-Muñiz thank the University of Oviedo for the "Plan de Apoyo y Promoción de la Investigación" grant (PAPI-18-PF-13) and the "Ayudas Proyectos Emergentes 2019" project (PAPI-19-EMERG-17) respectively. C. Toyos-Rodríguez thanks the MICINN for the award of a FPI Grant (PRE2018-084953). A. de la Escosura-Muñiz also acknowledges the MICINN for the "Ramón y Cajal" Research Fellow (RyC-2016-20299). The authors acknowledge the Chronic Ulcers Unit of the Hospital Universitario Central de Asturias (HUCA) and specially to Prof. Víctor Asensi and Susana Valerdiz for providing the real samples used in this work.

Appendix A. Supplementary data

Supplementary data related to this article can be found at https://doi.org/10.1016/j.bios.2022.114243.

References

Caliendo, A.M., Gilbert, D.N., Ginocchio, C.C., Hanson, K.E., May, L., Quinn, T.C., Tenover, F.C., Alland, D., Blaschke, A.J., Bonomo, R.A., Carroll, K.C., Ferraro, M.J., Hirschhorn, L.R., Joseph, W.P., Karchmer, T., MacIntyre, A.T., Reller, L.B., Jackson, A.F., 2013. Better tests, better care: improved diagnostics for infectious diseases. Clin. Infect. Dis. 57, S139–S170. https://doi.org/10.1093/cid/cit578.

Callewaert, L., Michiels, C.W., 2010. Lysozymes in the animal kingdom. J. Biosci. 35, 127–160. https://doi.org/10.1007/s12038-010-0015-5.

Clarke, J., Wu, H.C., Jayasinghe, L., Patel, A., Reid, S., Bayley, H., 2009. Continuous base identification for single-molecule nanopore DNA sequencing. Nat. Nanotechnol. 4, 265–270. https://doi.org/10.1038/nnano.2009.12.

Clinton, A., Carter, T., 2015. Chronic wound biofilms: pathogenesis and potential therapies. Lab. Med. 46, 277–284. https://doi.org/10.1309/LMBNSWKUI4JPN7SO.

Cutting, K.F., White, R.J., 2005. Criteria for identifying wound infection-revisited. Ostomy/Wound Manag. 51, 28–34.

de la Escosura-Muñiz, A., Chunglok, W., Surareungchai, W., Merkoçi, A., 2013. Nanochannels for diagnostic of thrombin-related diseases in human blood. Biosens. Bioelectron. 40, 24–31. https://doi.org/10.1016/j.bios.2012.05.021.

de la Escosura-Muñiz, A., Espinoza-Castañeda, M., Chamorro-García, A., Rodríguez-Hernández, C.J., de Torres, C., Merkoçi, A., 2018. In situ monitoring of PTHLH secretion in neuroblastoma cells cultured onto nanoporous membranes. Biosens. Bioelectron. 107, 62–68. https://doi.org/10.1016/j.bios.2018.01.064.

de la Escosura-Muniz, A., Ivanova, K., Tzanov, T., 2019. Electrical evaluation of bacterial virulence factors using nanopores. ACS Appl. Mater. Interfaces 11, 13140–13146. https://doi.org/10.1021/acsami.9b02382.

de la Escosura-Muñiz, A., Merkoçi, A., 2016. Nanochannels for electrical biosensing. TrAC Trends Anal. Chem. (Reference Ed.) 79, 134–150. https://doi.org/10.1016/j.trac.2015.12.003.

de la Escosura-Muñiz, A., Merkoçi, A., 2012. Nanochannels preparation and application in biosensing. ACS Nano 6, 7556–7583. https://doi.org/10.1021/nn301368z.

de la Escosura-Muñiz, A., Merkoçi, A., 2011. A nanochannel/nanoparticle-based filtering and sensing platform for direct detection of a cancer biomarker in blood. Small 7, 675–682. https://doi.org/10.1002/smll.201002349.

Espinoza-Castañeda, M., Escosura-Muñiz, A. de la, Chamorro, A., Torres, C. de, Merkoçi, A., 2015. Nanochannel array device operating through Prussian blue nanoparticles for sensitive label-free immunodetection of a cancer biomarker. Biosens. Bioelectron. 67, 107–114. https://doi.org/10.1016/j.bios.2014.07.039.

Fang, X., Wang, Z., Sun, N., Deng, C., 2021. Magnetic metal oxide affinity chromatography-based molecularly imprinted approach for effective separation of serous and urinary phosphoprotein biomarker. Talanta 226, 122143. https://doi.org/10.1016/j.talanta.2021.122143.

Fu, F., Li, L., Luo, Q., Li, Q., Guo, T., Yu, M., Song, Y., Song, E., 2018. Selective and sensitive detection of lysozyme based on plasmon resonance light-scattering of hydrolyzed peptidoglycan stabilized-gold nanoparticles. Analyst 143, 1133–1140. https://doi.org/10.1039/c7an01570d.

Gao, H.L., Zhang, H., Li, C.Y., Xia, X.H., 2013. Confinement effect of protonation/deprotonation of carboxylic group modified in nanochannel. Electrochim. Acta 110, 159–163. https://doi.org/10.1016/j.electacta.2012.12.080.

Gardner, S.E., Frantz, R.A., Doebbeling, B.N., 2001. The validity of the clinical signs and symptoms used to identify localized chronic wound infection. Wound Repair Regen. 9, 178–186. https://doi.org/10.1046/j.1524-475X.2001.00178.x.

Gardner, S.E., Frantz, R.A., Saltzman, C.L., Hillis, S.L., Park, H., Scherubel, M., 2006. Diagnostic validity of three swab techniques for identifying chronic wound infection. Wound Repair Regen. 14, 548–557. https://doi.org/10.1111/j.1743-6109.2006.00162.x.

Hardt, M., Guo, Y., Henderson, G., Laine, R.A., 2003. Zymogram with remazol brilliant blue-labeled Micrococcus lysodeikticus cells for the detection of lysozymes: example of a new lysozyme activity in Formosan termite defense secretions. Anal. Biochem. 312, 73–76. https://doi.org/10.1016/S0003-2697(02)00443-8.

Hasmann, A., Wehrschuetz-Sigl, E., Kanzler, G., Gewessler, U., Hulla, E., Schneider, K.P., Binder, B., Schintler, M., Guebitz, G.M., 2011. Novel peptidoglycan-based diagnostic devices for detection of wound infection. Diagn. Microbiol. Infect. Dis. 71, 12–23. https://doi.org/10.1016/j.diagmicrobio.2010.09.009.

Ito, Y., Yamada, H., Imoto, T., 1992. Colorimetric assay for lysozyme using Micrococcus luteus labeled with a blue dye, remazol brilliant blue R, as a substrate. Chem. Pharm. Bull. 40, 1523–1526.

Jain, R., Yadav, D., Puranik, N., Guleria, R., Jin, J.-O., 2020. Sarcoidosis: causes, diagnosis, clinical features, and treatments. J. Clin. Med. 9, 1081. https://doi.org/10.3390/jcm9041081.

Järbrink, K., Ni, G., Sönnergren, H., Schmidtchen, A., Pang, C., Bajpai, R., Car, J., 2016. Prevalence and incidence of chronic wounds and related complications: a protocol for a systematic review. Syst. Rev. 5, 152. https://doi.org/10.1186/s13643-016-0329-y.

Li, C.Y., Ma, F.X., Wu, Z.Q., Gao, H.L., Shao, W.T., Wang, K., Xia, X.H., 2013. Solution-pH-modulated rectification of ionic current in highly ordered nanochannel arrays patterned with chemical functional groups at designed positions. Adv. Funct. Mater. 23, 3836–3844. https://doi.org/10.1002/adfm.201300315.

Li, C.Y., Tian, Y.W., Shao, W.T., Yuan, C.G., Wang, K., Xia, X.H., 2014. Solution pH regulating mass transport in highly ordered nanopore array electrode. Electrochem. Commun. 42, 1–5. https://doi.org/10.1016/j.elecom.2014.01.020.

Li, C.Y., Wu, Z.Q., Yuan, C.G., Wang, K., Xia, X.H., 2015. Propagation of concentration polarization affecting ions transport in branching nanochannel array. Anal. Chem. 87, 8194–8202. https://doi.org/10.1021/acs.analchem.5b01016.

Li, S., Li, J., Wang, K., Wang, C., Xu, J., Chen, H., Xia, X., Huo, Q., States, U., 2010. A nanochannel array-based electrochemical device for quantitative label-free DNA analysis. ACS Nano 4, 6417–6424.

Losic, D., Santos, A., 2015. Nanoporous Alumina: Fabrication, Structure, Properties and Applications. Springer Series in Materials Science. https://doi.org/10.1007/978-3-319-20334-8_5.

Matzeu, G., Losacco, M., Parducci, E., Pucci, A., Dini, V., Romanelli, M., Di Francesco, F., 2011. Skin temperature monitoring by a wireless sensor. IECON Proc. (Industrial Electron. Conf. 3533–3535. https://doi.org/10.1109/IECON.2011.6119881.

Mörsky, P., 1983. Turbidimetric determination of lysozyme with Micrococcus lysodeikticus cells: reexamination of reaction conditions. Anal. Biochem. 128, 77–85. https://doi.org/10.1016/0003-2697(83)90347-0.

Osserman, E.F., Klockars, M., Halper, J., Fischel, R.E., 1973. Effects of lysozyme on normal and transformed mammalian cells. Nature 243, 331–335. https://doi.org/10.1038/246421a0.

Osserman, E.F., Lawlor, D.P., 1966. Serum and urinary lysozyme (muramidase) in monocytic and monomyelocytic leukemia. J. Exp. Med. 125, 921–952.

Ostatná, V., Kasalová-Vargová, V., Kékedy-Nagy, L., Černocká, H., Ferapontova, E.E., 2017. Chronopotentiometric sensing of specific interactions between lysozyme and the DNA aptamer. Bioelectrochemistry 114, 42–47. https://doi.org/10.1016/j.bioelechem.2016.12.003.

Persaud, K.C., 2005. Medical applications of odor-sensing devices. Int. J. Low. Extrem. Wounds 4, 50–56. https://doi.org/10.1177/1534734605275139.

Rogers, H.J., Perkins, H.R., Ward, J.B., 2013. Microbial Cell Walls and Membranes. Springer.

Salton, M.R.J., 1957. The properties of lysozyme and its action on microorganisms. Bacteriol. Rev. 21, 82–100. https://doi.org/10.1128/mmbr.21.2.82-100.1957.

Sambrook, J., Fritsch, E.F., Maniatis, T., 1989. Molecular Cloning: A Laboratory Manual. Cold Spring Harbor, 1989. Cold Spring Harbor Laboratory, New York.

Schiffer, D., Tegl, G., Heinzle, A., Sigl, E., Metcalf, D., Bowler, P., Burnet, M., Guebitz, G. M., 2015. Enzyme-responsive polymers for microbial infection detection. Expert Rev. Mol. Diagn. 15, 1125–1131. https://doi.org/10.1586/14737159.2015.1061935.

Shugar, D., 1952. The measurement of lysozyme activity and the ultra-violet inactivation of lysozyme. Biochim. Biophys. Acta 8, 302–309. https://doi.org/10.1016/0006-3002(52)90045-0.

Siddiqui, A.R., Bernstein, J.M., 2010. Chronic wound infection: facts and controversies. Clin. Dermatol. 28, 519–526. https://doi.org/10.1016/j.clindermatol.2010.03.009.

Trupp, S., Alberti, M., Carofiglio, T., Lubian, E., Lehmann, H., Heuermann, R., Yacoub-George, E., Bock, K., Mohr, G.J., 2010. Development of pH-sensitive indicator dyes for the preparation of micro-patterned optical sensor layers. Sensor. Actuator. B Chem. 150, 206–210. https://doi.org/10.1016/j.snb.2010.07.015.

Tulum, I., Tahara, Y.O., Miyata, M., 2019. Peptidoglycan layer and disruption processes in Bacillus subtilis cells visualized using quick-freeze, deep-etch electron microscopy. Microscopy 68, 441–449. https://doi.org/10.1093/jmicro/dfz033.

Vidal, M.-L., Gautron, J., Nys, Y., 2005. Development of an ELISA for quantifying lysozyme in hen egg white. J. Agric. Food Chem. 53, 2379–2385. https://doi.org/10.1021/jf048692o.

Vollmer, W., Blanot, D., de Pedro, M.A., 2008. Peptidoglycan structure and architecture. FEMS Microbiol. Rev. 32, 149–167. https://doi.org/10.1111/j.1574-6976.2007.00094.x.

Wang, C., Liu, H.L., Li, Y.Q., Cao, J., Zheng, B., Xia, X.H., Feng, F., 2016. A novel device of array nanochannels integrated electrochemical detector for detection of amyloid β aggregation and inhibitor screening. Electrochem. Commun. 66, 25–28. https://doi.org/10.1016/j.elecom.2016.02.016.

Wang, C., Xu, J., Chen, H., Xia, X., 2012. Mass transport in nanofluidic devices. Sci. China Chem. 55, 453–468. https://doi.org/10.1007/s11426-012-4542-9.

Yager, D.R., Kulina, R.A., Gilman, L.A., 2007. Wound fluids: a window into the wound environment? Int. J. Low. Extrem. Wounds 6, 262–272. https://doi.org/10.1177/1534734607307035.

Ye, W., Xu, Y., Zheng, L., Zhang, Y., Yang, M., Sun, P., 2016. A nanoporous alumina membrane based electrochemical biosensor for histamine determination with biofunctionalized magnetic nanoparticles concentration and signal amplification. Sensors 16, 1767. https://doi.org/10.3390/s16101767.

Yoshida, H., Kinoshita, K., Ashida, M., 1996. Purification of a peptidoglycan recognition protein from hemolymph of the silkworm, Bombyx mori. J. Biol. Chem. 271, 13854–13860. https://doi.org/10.1074/jbc.271.23.13854.

Yu, J., Zhang, L., Xu, X., Liu, S., 2014. Quantitative detection of potassium ions and adenosine triphosphate via a nanochannel-based electrochemical platform coupled with G-quadruplex aptamers. Anal. Chem. 86, 10741–10748. https://doi.org/10.1021/ac502752g.

Zhao, X.P., Zhou, Y., Zhang, Q.W., Yang, D.R., Wang, C., Xia, X.H., 2019. Nanochannel-ion channel hybrid device for ultrasensitive monitoring of biomolecular recognition events. Anal. Chem. 91, 1185–1193. https://doi.org/10.1021/acs.analchem.8b05162.

Zhou, Y., Liao, X., Han, J., Chen, T., Wang, C., 2020. Ionic current rectification in asymmetric nanofluidic devices. Chin. Chem. Lett. 31, 2414–2422. https://doi.org/10.1016/j.cclet.2020.05.033.